Atmos. Chem. Phys., 15, 883–897, 2015
www.atmos-chem-phys.net/15/883/2015/
doi:10.5194/acp-15-883-2015


Atmospheric Chemistry and Physics Open Access

# Aging of secondary organic aerosol generated from the ozonolysis of $\alpha$-pinene: effects of ozone, light and temperature

**C. Denjean[1,2], P. Formenti[1], B. Picquet-Varrault[1], M. Camredon[1], E. Pangui[1], P. Zapf[1], Y. Katrib[1], C. Giorio[3,*], A. Tapparo[3], B. Temime-Roussel[4], A. Monod[4], B. Aumont[1], and J. F. Doussin[1]**

[1]Laboratoire Interuniversitaire des Systèmes Atmosphériques (LISA), UMR-CNRS 7583, Université Paris-Est-Créteil (UPEC) et Université Paris Diderot (UPD), Institut Pierre Simon Laplace (IPSL), Créteil, France
[2]Leibniz Institute for Tropospheric Research (TROPOS), Permoserstr. 15, 04318 Leipzig, Germany
[3]Dipartimento di Scienze Chimiche, Università degli Studi di Padova, Via Marzolo 1, 35131 Padova, Italy
[4]Aix Marseille Université, CNRS, LCE FRE 3416, 13331 Marseille, France
[*]now at: Department of Chemistry, University of Cambridge, Lensfield Road, CB2 1EW Cambridge, UK

*Correspondence to:* C. Denjean (denjean@tropos.de)

Received: 18 July 2014 – Published in Atmos. Chem. Phys. Discuss.: 1 September 2014
Revised: 4 December 2014 – Accepted: 19 December 2014 – Published: 26 January 2015

**Abstract.** A series of experiments was conducted in the CESAM (French acronym for Experimental Multiphasic Atmospheric Simulation Chamber) simulation chamber to investigate the evolution of the physical and chemical properties of secondary organic aerosols (SOAs) during different forcings. The present experiments represent a first attempt to comprehensively investigate the influence of oxidative processing, photochemistry, and diurnal temperature cycling upon SOA properties. SOAs generated from the ozonolysis of $\alpha$-pinene were exposed under dry conditions (< 1 % relative humidity) to (1) elevated ozone concentrations, (2) light (under controlled temperature conditions) or (3) light and heat (6 °C light-induced temperature increase), and the resultant changes in SOA optical properties (i.e. absorption and scattering), hygroscopicity and chemical composition were measured using a suite of instrumentation interfaced to the CESAM chamber. The complex refractive index (CRI) was derived from integrated nephelometer measurements of 525 nm wavelength, using Mie scattering calculations and measured number size distributions. The particle size growth factor (GF) was measured with a hygroscopic tandem differential mobility analyzer (H-TDMA). An aerosol mass spectrometer (AMS) was used for the determination of the $f_{44}$ / $f_{43}$ and O : C ratio of the particles bulk.

No change in SOA size or chemical composition was observed during $O_3$ and light exposure at constant temperature; in addition, GF and CRI of the SOA remained constant with forcing. On the contrary, illumination of SOAs in the absence of temperature control led to an increase in the real part of the CRI from 1.35 (±0.03) to 1.49 (±0.03), an increase of the GF from 1.04 (±0.02) to 1.14 (±0.02) and an increase of the $f_{44}$ / $f_{43}$ ratio from 1.73 (±0.03) to 2.23 (±0.03). The simulation of the experiments using the master chemical mechanism (MCM) and the Generator for Explicit Chemistry and Kinetics of Organics in the Atmosphere (GECKO-A) shows that these changes resulted from the evaporation of semi-volatile and less oxidized SOA species induced by the relatively minor increases in temperature (∼ 6 °C). These surprising results suggest that $\alpha$-pinene–$O_3$ SOA properties may be governed more by local temperature fluctuations than by oxidative processing and photochemistry.

## 1 Introduction

Atmospheric aerosols influence climate directly by altering the absorption and scattering of solar and terrestrial radiation (Haywood and Ramaswamy, 1998) and indirectly by changing cloud properties (Lohmann and Feichter, 2005). One of the major uncertainties in estimating the aerosol radiative effect is associated with the contribution of secondary organic aerosols (SOAs). SOAs are formed by condensation of species formed during gas-phase oxidation of volatile organic compounds (VOCs) and are a major constituent of at-

mospheric organic aerosol Kanakidou et al., 2005; Turpin and Huntzicker, 1995; Zhang et al., 2007). During their atmospheric lifetime, which ranges from 48 to 72 h (Wagstrom and Pandis, 2009), their physical and chemical properties do not stay constant but rather evolve in response to local atmospheric conditions. For example, studies have shown that SOAs can grow by condensation of low volatility oxidized species (Ellison et al., 1999) and by cloud processing (Cocker et al., 2001; Ervens and Volkamer, 2010; Volkamer et al., 2009). SOAs can also be oxidized by gas-phase oxidants (Kalberer, 2004; Gao et al., 2004), undergo chemical reactions in the particle phase (Kalberer, 2004; Gao et al., 2004) or partially evaporate (Warren et al., 2009). These changes in aerosol properties have also been observed in the field; for example, more oxidized, less volatile and more hygroscopic SOAs are typically observed in remote areas as a result of continuous aging in the atmosphere (Jimenez et al., 2009; Ng et al., 2011; Rudich et al., 2007). Since SOA contains a wide variety of organic compounds, which vary in terms of their size, structure, functionality and oxidation state (Kroll and Seinfeld, 2008; Jimenez et al., 2009; de Gouw et al., 2005; Hallquist et al., 2009), the processes associated with SOA aging are very complex.

Experiments performed in simulation chambers have significantly improved our understanding of the SOA aging processes (Donahue et al., 2012; Qi et al., 2012; Yasmeen et al., 2012). In order to provide modellers with accurate parameters for SOA aging in the atmosphere, these experiments must be atmospherically relevant (Kourtchev et al., 2014). While the O : C ratio of laboratory-generated SOAs is similar to that of freshly formed ambient SOAs, it is generally lower than that of aged ambient SOAs (Ng et al., 2010). In addition, while the representation of SOAs in chemical transport models based on parameterization of chamber data showed a good agreement with nighttime SOA concentrations (in a rural site near Rotterdam, the Netherlands), an underprediction of SOA concentrations occurred during the day (Li et al., 2013).

Research has shown that the oxidative aging of SOAs in the atmosphere has a major influence on its properties. For example, studies have shown that highly oxygenated organic particles are likely to have a higher hygroscopicity and cloud condensation nuclei (CCN) activity than freshly emitted particles, due to the increased polarity and solubility of their constituents (Massoli et al., 2010; Jimenez et al., 2009; Chang et al., 2010; Duplissy et al., 2011). Oxidative aging has also been shown to lead to changes in the real part of the complex refractive index (CRI) of SOAs (Cappa et al., 2011; Lambe et al., 2013; Flores et al., 2014), and to an increase in its UV absorption via the formation of additional carbonyl compounds and oligomeric products (Sareen et al., 2013; Nozière and Esteve, 2005; Shapiro et al., 2009; Lambe et al., 2013). To date, laboratory studies have primarily focused on oxidative aging mediated by the heterogeneous reactive uptake of OH radical (Rudich et al., 2007; George and Abbatt, 2010; Smith et al., 2009). On the other hand, oxidative aging by $O_3$ has received less attention.

Light exposure has also been shown to influence SOA properties; through photodissociation of molecules, such as carbonyls and organic peroxides, either in the gas or the particle phase, it has been shown to induce a decrease in SOA mass concentration (Kroll et al., 2006; Bateman et al., 2011). There are also indications of significant photolytic processing of carbonyl compounds in aerosols during long-range transport (Hawkins and Russell, 2010). In addition, laboratory studies have revealed that photochemical processes alter the chemical composition of SOAs (Tritscher et al., 2011; Cappa et al., 2011; Qi et al., 2012; George and Abbatt, 2010; Donahue et al., 2012) and modify its hydrophilicity (Tritscher et al., 2011; George and Abbatt, 2010; George et al., 2009), optical properties (Cappa et al., 2011) and volatility (Tritscher et al., 2011). In these studies, $H_2O_2$ was used as a photolytic OH precursor. Since this OH source requires the use of UV light, these experiments did not allow for the individual effects of heterogeneous reactions by OH and direct photolysis on SOA properties to be distinguished.

SOA properties can also be affected by local temperature variations via the evaporation of volatile products. A number of studies have used thermodenuder-based techniques to investigate the volatility of SOAs and to determine the effect of temperature on SOA properties (Asa-Awuku et al., 2008; Huffman et al., 2009; Cappa and Wilson, 2011). Volatile tandem differential mobility analyzers (V-TDMAs) have been used to measure the shrinkage of monodisperse particles after heating (Cappa and Wilson, 2011; Salo et al., 2011). In these studies, particles were exposed to elevated temperatures (up to 300 °C) for a short time. It has been shown, however, that SOA exhibits a significantly slower response to changes in temperature than that predicted by models for liquid droplets (Cappa and Wilson, 2011). Recently, it has been suggested that SOA could be in an amorphous semi-solid or amorphous solid (glassy) state under dry conditions (Renbaum-Wolff et al., 2013; Saukko et al., 2012; Denjean et al., 2014b), which could limit the volatilization kinetics of the aerosol.

This study focuses on the SOA formed from the ozonolysis of $\alpha$-pinene, which is an important source of SOAs on both regional and global scales (Guenther et al., 1995; Hallquist et al., 2009). In our companion paper (Denjean et al. 2014b), we explored the evolution of the physical, chemical, optical and hygroscopic properties of $\alpha$-pinene–$O_3$ SOAs during the first hours after its formation. However, Wang et al. (2011) have shown that particle lifetime can vary from 10 h to 4 days in the CESAM simulation chamber. CESAM is a powerful tool for the study of SOAs over longer timescales corresponding to their lifetime in the atmosphere (Yasmeen et al., 2012). In the present work, we investigate in the same chamber the effects of (i) additional ozone exposure, (ii) light exposure and (iii) temperature variation on the chemical composition, hygroscopicity and optical properties of $\alpha$-pinene–$O_3$ SOA, over timescales reaching 20 h.

## 2 Methods

### 2.1 CESAM atmospheric simulation chamber

The present experiments were performed in the CESAM (French acronym for Experimental Multiphasic Atmospheric Simulation Chamber) atmospheric simulation chamber, which has previously been described in detail by Wang et al. (2011). In brief, CESAM is a stainless-steel chamber with a volume of 4.2 $m^3$. Chamber illumination is accomplished using the borosilicate-filtered output of three high-pressure arc xenon lamps (4 kW, XPO 4000 W/HS, OSRAM), which provides a good reproduction of the solar energy distribution at the Earth's surface over the 290–700 nm wavelength region. The inner walls of the chamber are polished in order to provide good reflection inside the chamber and thus enhance the radiation homogeneity. During our experiments, the $NO_2$ photolysis frequency $J_{NO_2}$ within the chamber was approximately $3 \times 10^{-3}\,s^{-1}$, which corresponds to a solar zenith angle of $\sim 70°$ (Carter et al., 2005). The simulation chamber was maintained at room temperature ($\pm 1\,°C$) using a refrigerating liquid (70 % water / 30 % ethylene glycol), which was circulated in the double walls of the chamber. Temperature and relative humidity (RH) are monitored with a transmitter (HMP234, Vaisala) equipped with a thin-film capacitive humidity sensor (HUMICAP®, Vaisala). During our experiments, the temperature accuracy is $\pm 0.1\,°C$ at 20 °C and the RH accuracy is $\pm 1.9$ % (up to 90 % RH).

### 2.2 Experimental details

Prior to each experiment, the chamber was evacuated to a secondary vacuum (typical pressure $\sim 4 \times 10^{-4}$ mbar) and kept under vacuum overnight. The chamber was then filled to atmospheric pressure with a mixture of 200 mbar of oxygen (Air Liquide, ALPHAGAZ™ class 1, purity 99.9 %) and 800 mbar of nitrogen produced from the evaporation of a pressurized liquid nitrogen tank (Messer, purity > 99.995 %, $H_2O$ < 5 ppm). The background conditions were typically: particles concentration $< 0.1\,\mu g\,m^{-3}$, ozone mixing ratio < 5 ppb, gas-phase organics < 5 ppb and RH < 1 %. To avoid contamination, a slight overpressure of about 5 mbar with respect to the atmospheric pressure was maintained during each experiment by adding nitrogen (Messer, purity > 99.995 %, $H_2O$ < 5 ppm).

All aging experiments were carried out under the same initial conditions with $\alpha$-pinene and ozone reacting in the dark, with neither seeds nor OH scavenger. $O_3$ was generated in an $O_2$ flow using a commercial dielectric ozone SOA generator (MBT 802N, Messtechnik GmbH, Stahnsdorf, Germany) and introduced to the chamber through an injection port. Quantification of $\alpha$-pinene was performed by evaporating precisely measured amounts of the terpene into a glass bulb held under vacuum. When the $O_3$ concentration within the chamber reached $\sim 250$ ppb, $\alpha$-pinene (Aldrich, 98 %) was flushed from the bulb into the chamber in a flow of oxygen to a concentration of $\sim 200$ ppb within the chamber. In all experiments, SOAs, formed directly after $\alpha$-pinene injection, and its precursors were essentially consumed after 4 h of reaction.

In our companion paper, we observed changes in the oxidative degree and optical properties during the formation of SOAs, but these changes ceased after 9 h of reaction (Denjean et al., 2014b). In the present study, therefore, SOAs were allowed to evolve for 14 h prior to simulating atmospheric processing, which was in turn conducted over a period of 6 h. Three different aging regimes were applied after 14 h of $\alpha$-pinene ozonolysis: (1) 700 ppb of ozone was introduced into the simulation chamber, (2) SOAs were exposed to light for 6 h in the absence of temperature control, during which time the temperature increased by $\sim 6\,°C$ and (3) SOAs were exposed to light for 6 h under controlled temperature conditions ($\pm 1\,°C$). For comparison purposes, control experiments were performed: in these experiments, SOAs were allowed to remain in the chamber for 20 h under dark conditions. The specific experimental conditions associated with each aging regime are shown in Table 1. As discussed in our companion paper (Denjean et al., 2014b), the variation of SOA mass concentration between the experiments was attributed to different concentrations of $\alpha$-pinene injected to the chamber. Despite this, the chemical, optical and hygroscopic properties of SOA were found to be very similar between the experiments. Therefore, the experiments were considered to be comparable for studying the effect of forcing on SOA properties.

During these experiments, the concentrations of $\alpha$-pinene, ozone and VOCs were monitored using a Fourier transform infrared spectrometer (FTIR) from Bruker GmbH (Ettlingen, Germany) coupled to a multi-reflection cell with an optical path of 192 m. During the different forcings, the concentrations of gas-phase compounds were found to be below the detection limit. Ozone was also measured with a commercial instrument (Horiba APOA 370, Kyoto, Japan), with a detection limit of 0.2 ppb and a precision of 0.1 ppb.

### 2.3 Measurement of SOA properties

#### 2.3.1 Size distribution

SOA number size distributions between 14 and 505 nm were monitored using a scanning mobility particle sizer (SMPS; DMA Model 3080, CPC Model 3010; TSI) operated at flow rates of 3/0.3 Lpm (sheath flow/aerosol sample flow). Instrument calibration was conducted using polystyrene latex spheres (PSL) (Duke Scientific). Since the PSL diameters measured during calibration were $\sim 10$ % larger than the certified PSL diameters (for 100 nm PSL samples), a correction factor was applied to all measurements. Corrections for particle loss by diffusion in the SMPS tubing and the contribution of multiply charged particles were made using the SMPS

**Table 1.** Summary of experimental conditions.

| Type of forcing | Run | Forcing details | | | |
|---|---|---|---|---|---|
| | | $Cm_{t=0}$[a] $\mu g\,m^{-3}$ | $[O_3]_{t=0}$[b] (ppb) | Lights on (min) | $T_{t=0}/T_{t=6\,h}$[c] (°C) |
| Control experiments | E160411 | 50.4 | 0 | 0 | 20.5/22.3 |
| | E260411 | 112.5 | 0 | 0 | 20.4/21.3 |
| | E301111 | 36.5 | 0 | 0 | 18.4/18.9 |
| | E091211 | 42.5 | 0 | 0 | 17.2/18.3 |
| $O_3$ exposure | E021211 | 57.8 | 680 | 0 | 18.1/17.7 |
| | E071211 | 48.1 | 630 | 0 | 17.1/16.9 |
| Light exposure with increasing temperature | E200411 | 78.0 | 0 | 348 | 21.4/27.9 |
| | E281111 | 29.8 | 0 | 358 | 17.2/23.2 |
| | E051211 | 50.5 | 0 | 346 | 16.4/22.7 |
| | E120312 | 117 | 0 | 350 | 20.7/25.4 |
| Light exposure | E030512 | 80.0 | 0 | 354 | 21.4/21.9 |
| | E060512 | 84 | 0 | 361 | 19.8/20.1 |

[a] Aerosol mass concentration estimated from the aerosol volume concentration corrected from dilution and by assuming a density of $1.2\,g\,cm^{-3}$.
[b] Ozone concentrations determined using FTIR spectroscopy.
[c] Temperature before forcing/temperature after forcing.

software (Aerosol Instrument Manager, version 9, TSI). The number size distribution was used to obtain SOA mass concentrations, assuming homogeneous spherical particles and an effective density of $1.2\,g\,m^{-3}$, as determined by Shilling et al. (2008), Saathoff et al. (2009) and Denjean et al. (2014b).

### 2.3.2 Chemical composition

SOA chemical composition was analyzed using a high-resolution time-of-flight aerosol mass spectrometer (HR-ToF-AMS, Aerodyne) (DeCarlo et al., 2006). Instrumental and data treatment details are given in our companion paper (Denjean et al., 2014b), and thus will be described only briefly here. The HR-ToF-AMS was used under standard conditions (vaporizer at 600 °C and electron ionization at 70 eV). The instrument was switched between two modalities: a single-reflectron configuration (V-mode), which offers higher sensitivity but lower resolving power (up to $\sim$ 2100 at $m/z$ 200), and a double-reflectron configuration (W-mode), which provides a higher resolving power (up to $\sim$ 4300 at $m/z$ 200) but a lower sensitivity (De Carlo et al., 2006). Default collection efficiencies (CEs) and relative ionization efficiencies (RIEs) were used for quantification of SOA composition. High-resolution analysis was performed using V-mode data, by integrating each $C_xH_yO_z$ ion in the mass range 12–180 $m/z$; W-mode data were used only to check for possible interferences. The method is based on the RIEs of molecules containing C, H and O atoms. The sum of the ion signal intensities from all fragments was used to estimate the O : C ratio of the SOA, and thus its degree of oxidation. Air interferences were removed by adjusting the fragmentation table (Aiken et al., 2007; Allan et al., 2004). Additional modification of the fragmentation table was made for organic $H_2O^+$ as suggested by Chen et al. (2011). The default fragmentation table derives the contribution from fragmentation of organic compounds (dehydration) to the ion $H_2O^+$ as organic $H_2O^+ = 0.225^* CO_2^+$, considering that the measured excess is due to the interference of water. Since the experiments were run under very dry conditions (RH < 1 %), the ion $H_2O^+$ has been totally assigned to fragmentation of organic compounds which corresponds to a organic $H_2O^+$ to $CO_2^+$ ratio of 0.8–1:1. Similar organic $H_2O^+$ to $CO_2^+$ were obtained in previous studies of $\alpha$-pinene ozonolysis (Chen et al., 2011; Chhabra et al., 2010). Measurement uncertainties of O : C were estimated to be $\pm$30 %, as determined by Aiken et al (2007).

### 2.3.3 Optical properties

SOA optical properties were characterized by combining data obtained from an integrating nephelometer (Model M9003, Ecotech), a spectral aethalometer (Model AE31, Magee Scientific) and the SMPS described above. The integrating nephelometer measured the scattering coefficient ($\sigma_{scatt}$) of 525 nm wavelength, as well as the temperature and relative humidity of the incoming airflow, and was calibrated prior to the experiments using filtered air and $CO_2$. The nephelometer collected light only from particles at scattering angles between 10° and 170°. Measured scattering coefficients were corrected for this angular truncation using Mie calculations, which were performed using the measured SMPS size distribution. The aethalometer measured the SOA ab-

sorption coefficient at 7 wavelengths (370, 470, 520, 590, 660, 880 and 950 nm) by measuring the increase in attenuation of transmitted light through its quartz fiber filter as a function of particle exposure time. In order to avoid artefacts from the adsorption of ozone and VOCs on the filter, a charcoal denuder was installed upstream of the aethalometer (Weingartner et al., 2003). Measurements of light attenuation were corrected for aerosol scattering effects according to the method described by Collaud Coen et al. (2010) and using the parameters obtained by Denjean et al. (2014a, 2014b) for $\alpha$-pinene–$O_3$ SOAs.

These measurements were ultimately used to calculate the real and imaginary parts of the CRI, which together describe the scattering and absorbing characteristics of SOAs. The CRI retrieval procedure employed has been described and validated in Denjean et al. (2014a). In brief, the CRI of SOAs was retrieved at 525 nm by comparing the measured scattering and absorbing coefficients ($\sigma_{scat}$ and $\sigma_{abs}$,respectively) with those obtained from Mie scattering calculations (Bohren and Huffman, 1983) performed using the measured number size distribution. The absolute error associated with the real CRI was $\pm 0.03$ (Denjean et al., 2014b).

#### 2.3.4 Hygroscopic properties

SOA hygroscopic properties were analyzed with a custom-built hygroscopic tandem differential mobility analyzer (H-TDMA), which is described in detail in Denjean et al. (2014a). The first differential mobility analyzer (DMA) was used to select particles with a mobility diameter of 200 nm, which were then humidified at a constant RH of $90 \pm 1$ % (residence time $\sim 15$ s). The second DMA, which was coupled to a CPC, measured the humidified size distribution (with respect to the mobility diameter). Both DMAs were calibrated using monodisperse PSL particles (Duke Scientific) with size diameters of 70, 100, 200 and 300 and 500 nm. These size distributions were fitted to log-normal size distributions to obtain the dry geometric mean diameter, $D_{p,m}$ (dry), and the geometric mean diameter of the humidified aerosol, $D_{p,m}$ (90 % RH). These values were used to obtain the size growth factor (GF), which is defined as the ratio of $D_{p,m}$ (90 % RH) to $D_{p,m}$ (dry). The uncertainties in the calculated GF are associated with uncertainties in particle size distributions arising from DMA classification and calibration, as well as with uncertainties in the estimation of $D_{p,m}$ from size distributions, and are estimated to $\pm 0.02$. Prior to each experiment, the experimental set-up was validated by comparing measurements of the GF of ammonium sulfate particles to those predicted by Köhler theory (Denjean et al., 2014a).

### 2.4 Modelling SOA formation and aging

In order to assist in the interpretation of experimental results, the $\alpha$-pinene ozonolysis experiments were simulated using a box model that included the MCM (version 3.1) (Saunders et al., 2003) and the Generator for Explicit Chemistry and Kinetics of Organics in the Atmosphere (GECKO-A) (Aumont et al., 2005). The MCM v3.1 oxidation scheme for $\alpha$-pinene contains 329 organic species and 973 reactions. The GECKO-A chemical scheme for $\alpha$-pinene oxidation, which provides a more detailed description of the gaseous oxidation of organic species and takes into account minor reaction pathways not considered by the MCM, involves $5.7 \times 10^4$ organic species reacting according to $1.7 \times 10^6$ reactions (Valorso et al., 2011). Both models simulate gas–particle partitioning in terms of equilibria between the gas phase and an ideal liquid homogeneous condensed phase (Camredon et al., 2007).

Vapour pressures and boiling points for secondary organic species were estimated using the methods developed by Nannoolal et al. (2004, 2008), as they have been shown to provide the most reliable estimates for the purpose of SOA formation (Barley and McFiggans, 2010). Accretion, oxidation and photolysis in the condensed phase were not taken into account in this investigation in the models. In addition, recent studies (Renbaum-Wolff et al., 2013; Saukko et al., 2012; Denjean et al., 2014b) suggest that $\alpha$-pinene-$O_3$ SOA viscosity increases with aging. Due to possible kinetic limitations, heterogeneous chemistry and particle-phase reactions can be limited in highly viscous aerosol. The effect of viscosity on rate constants were not taken into account in the current MCM and Gecko-A models.

Time integration of the chemical schemes was solved using the two-step solver (Verwer et al., 1994, 1996). The gas–particle partitioning module was solved using the iterative method described in Pankow (2008). Simulations were initialized at a time point corresponding to $\alpha$-pinene injection. This injection was implemented in the model as a constant flux over the injection time period that reproduced the observed concentration. Dilution within the chamber (arising from the periodical injection of $N_2$ to compensate for instrumental sampling flows) was described as a measurement-constrained first-order process and applied in the simulations to both gas and aerosols. The temperature used in the simulations was that observed in the CESAM chamber during the experiments. Ozone-wall loss is significant in the CESAM chamber (Wang et al., 2011). The ozone loss rate employed in the simulations, therefore, was adjusted for each experiment in order to reproduce its measured decay.

## 3 Results

### 3.1 Changes in SOA size distribution during simulated atmospheric processing

Figure 1 shows the temporal evolution of SOA mass concentrations (normalized to the mass concentration at the beginning of each aging experiment and corrected for dilution

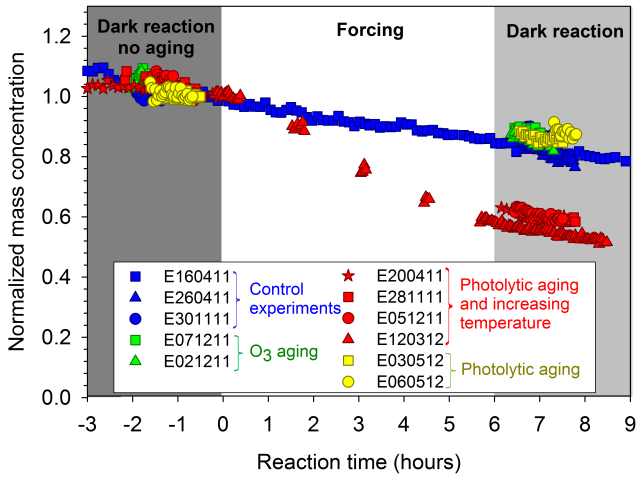


**Figure 1.** Temporal evolution of SOA mass concentrations (normalized to the mass concentration at the beginning of each forcing) during and after simulated atmospheric processing. In the control experiment (blue symbols), SOA was left to evolve in the chamber under dark conditions. In the $O_3$ aging experiments (green), SOA was exposed to an excess of ozone ($\sim$ 700 ppb) under constant temperature conditions. In the photochemical aging experiments, SOA was exposed to light for 6 h, either under constant temperature conditions (yellow) or with light-induced heating (red). Here, the initial time $t = 0$ corresponds to the beginning of simulated aging, which was commenced after SOA was allowed to form and stabilize for 14 h.

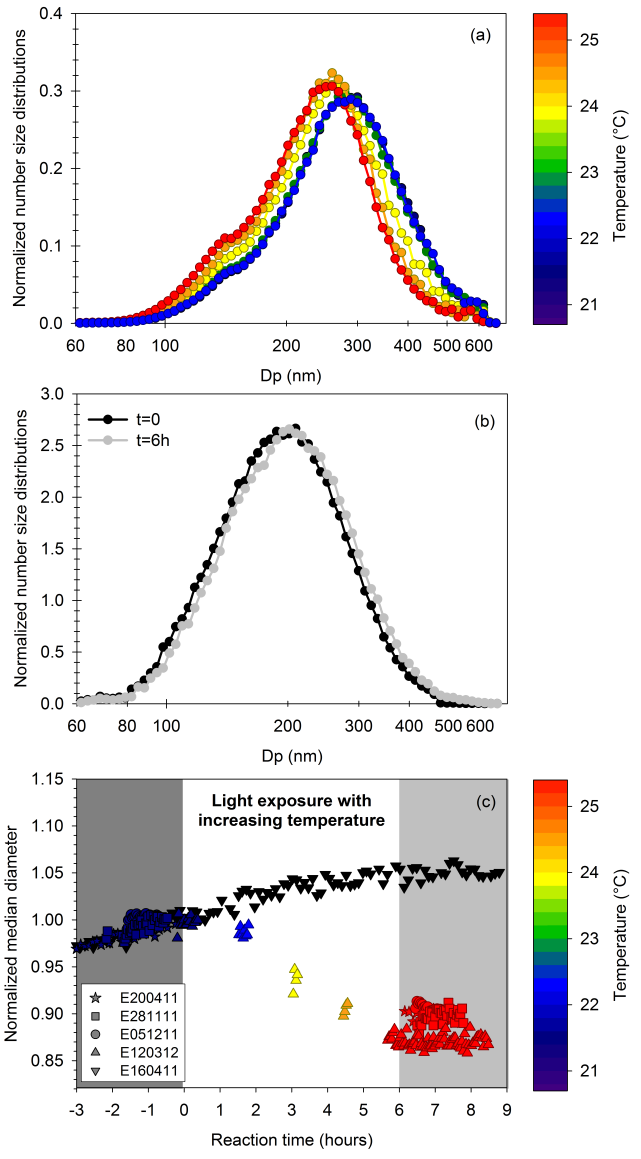


**Figure 2.** Temporal evolution of SOA number size distribution (normalized to the total number concentration) **(a)** during photochemical aging in the absence of temperature control (experiment E120312) and **(b)** during a control experiment (experiment E160411). The temporal evolution of the median diameter during photochemical aging in the absence of temperature control (experiments E201411, E281111, E051211 and E120312) and during a control experiment (Experiment E160411) is shown in **(c)**.

within the chamber) during and after simulated atmospheric processing. As shown in this figure, the SOA mass concentrations in the control experiments decreased by $\sim$ 15 % over the 6 h duration of the experiment. Since these measurements were performed after the total consumption of $O_3$, this mass decrease cannot be attributed to $O_3$-induced fragmentation reactions. It is thus probable that the SOA mass decrease observed in the control experiments arose via losses of particle and gaseous compounds to the chamber walls. Similar behaviour was observed when SOA was exposed to ozone and to light under controlled temperature conditions, which suggests that these forcings did not lead to significant fragmentation or functionalization. On the contrary, exposure of SOA to light and increasing temperature led to a 40 % loss in total SOA mass concentration and, as shown in Fig. 2, to a change in the SOA number size distribution: as the temperature increased from 20 °C to 26 °C, the geometric mean diameter of the normalized SOA number size distribution decreased from 286 nm to 249 nm, which also indicates that significant evaporation of SOA particles occurred.

### 3.2 Changes in SOA optical and hygroscopic properties during simulated atmospheric processing

Since the CRI is related to the aerosol chemical composition, density, molecular weight and polarization (Liu and Daum, 2008), it was thus expected to be influenced by atmospheric processing. The imaginary part of the SOA CRI over the 370–950 nm wavelength range is shown in Fig. 3. Its value was almost zero at all the wavelengths studied, which indicates that SOA, even after simulated atmospheric processing, has a pure scattering effect in the visible to near-UV region. The formation of chromophores has been observed previously from the ozonolysis of biogenic terpenes (Bones

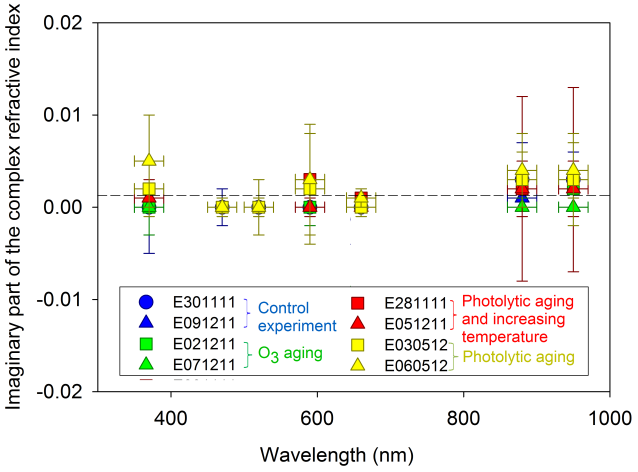


**Figure 3.** Wavelength dependence of the imaginary part of the complex refractive index of SOA before and after simulated atmospheric processing. In the control experiment (blue symbols), SOA was left to evolve in the chamber under dark conditions. In the $O_3$ aging experiments (green), SOA was exposed to an excess of ozone ($\sim$ 700 ppb) under constant temperature conditions. In the photochemical aging experiments, SOA was exposed to light for 6 h, either under constant temperature conditions (yellow) or with light-induced heating (red).

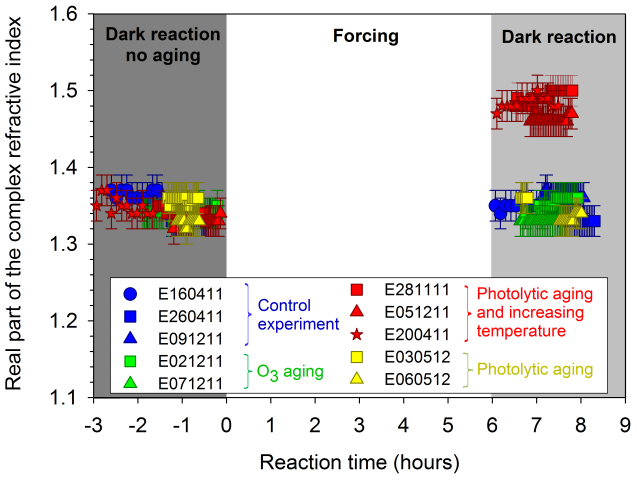


**Figure 4.** Measurements of the real part of the complex refractive index of SOA before and after simulated atmospheric processing. In the control experiment (blue symbols), SOA was left to evolve in the chamber under dark conditions. In the $O_3$ aging experiments (green), SOA was exposed to an excess of ozone ($\sim$ 700 ppb) under constant temperature conditions. In the photochemical aging experiments, SOA was exposed to light for 6 h, either under constant temperature conditions (yellow) or with light-induced heating (red). Here, the initial time t=0 corresponds to the beginning of simulated aging, which was commenced after SOA was allowed to form and stabilize for 14 h.

et al., 2010; Laskin et al., 2010; Zhong et al., 2012). Some oligomers formed in particle-phase can contain long conjugated structures which increase the light absorption properties of SOA in the visible. Interestingly, while one might have expected the formation of chromophores during the aging processes, our results indicate that this phenomenon occurred only weakly for $\alpha$-pinene–$O_3$ SOA and/or that the specific absorption of any potential aging products was not significant. Unlike toluene (Nakayama et al., 2010) or limonene (Bones et al., 2010), $\alpha$-pinene–$O_3$ SOA products did not contain long conjugated structures which absorbed visible radiation, at least under our experimental conditions when conducted in the absence of $NO_x$ or seed particles.

The influence of atmospheric processing upon the real part of the SOA CRI is shown in Fig. 4. No discernible change in real CRI was observed when the SOA was exposed to $O_3$ or to light at constant temperature. On the contrary, a significant increase in the real CRI was observed, 1.35 ($\pm$0.03) to 1.49 ($\pm$0.03), after photolytic forcing with increasing temperature. The hygroscopic properties of SOA were studied by measuring the GF at a constant relative humidity (90 $\pm$ 1 %). As shown in Fig. 5, the GF remained constant ($\sim$ 1.04 $\pm$ 0.02) both during $O_3$ exposure and during photochemical aging at constant temperature. These results are consistent with our observations of constant mass concentration and CRI of SOA, and confirm that no significant processing of the SOA occurred under these conditions. In contrast, a significant increase in the GF, from 1.04 ($\pm$0.02) to 1.14 ($\pm$0.02), was observed with increasing temperature.

### 3.3 Changes in SOA chemical composition during simulated atmospheric processing

The results presented in the previous two sections suggest that the exposure of the aging of SOA to light and increasing temperature resulted in changes in its physical, optical and hygroscopic properties, which are likely to be linked to changes in its chemical composition. Indeed, as shown in Fig. 6a, the increase in the O : C ratio of bulk SOA during its exposure to light and increasing temperature, 0.55 ($\pm$0.16) to 0.59 ($\pm$0.18), was much larger than that observed for SOA under control conditions. The increase in the O : C ratio was, however, within the measurement uncertainties ($\pm$30 %) estimated from Aiken et al. (2007). These uncertainties may be overestimated compared to the experimental variability and even experimental reproducibility observed in this study. In fact, we estimated the experimental uncertainties to be $\pm$0.01 from the standard deviation of the experimental values before the forcing. A new parameterization of the O : C ratio derived from the AMS was recently presented by Canagaratna et al. (2014). Application of this new parameterization to our measurements resulted in a O : C ratio similar to that obtained with our modified fragmentation table in which the measured fragment $H_2O^+$ was assigned to organic compounds. This indicates that the two methodologies agree under very dry conditions (RH < 1 %). The average O : C ratio obtained with both parameterizations was 20 % larger than that obtained

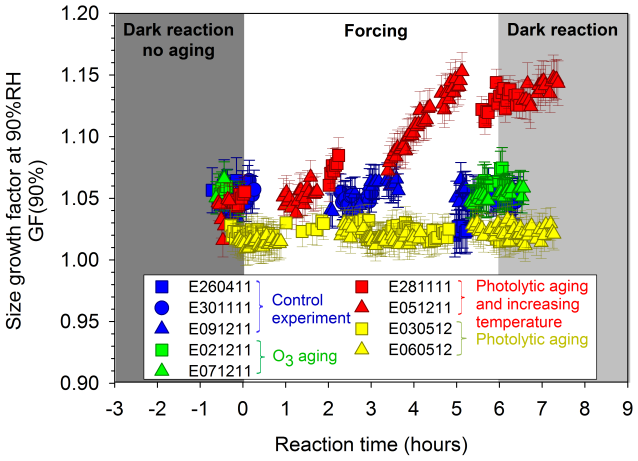


**Figure 5.** Temporal evolution of SOA hygroscopicity, here parameterized using the size growth factor (GF), during and after simulated atmospheric processing. In the control experiment (blue symbols), SOA was left to evolve in the chamber under dark conditions. In the $O_3$ aging experiments (green), SOA was exposed to an excess of ozone ($\sim$ 700 ppb) under constant temperature conditions. In the photochemical aging experiments, SOA was exposed to light for 6 h, either under constant temperature conditions (yellow) or with light-induced heating (red). Here, the initial time $t = 0$ corresponds to the beginning of simulated aging, which was commenced after SOA was allowed to form and stabilize for 14 h.

with the Aiken method and can be attributed to an underestimation in the Aiken method of the $CO^+$ and $H_2O^+$ ions produced from many oxidized species.

The fragments $f_{44}$, defined as the ratio of the $m/z$ 44 (a major fragment of organic acids and hydroperoxides) signal to the total organic aerosol signal, and $f_{43}$, defined as the ratio of $m/z$ 43 (associated with less oxygenated groups, e.g. aldehydes and alcohols) signal to the total organic aerosol signal, have been widely used in laboratory and field studies as indicators of SOA functionality and degree of oxidation (Ng et al., 2010; Alfarra et al., 2013; Poulain et al., 2010; Pfaffenberger et al., 2013). As shown in Fig. 6b, in the experiment performed under illumination but in the absence of temperature control, the $f_{44}$ / $f_{43}$ ratio of SOA increased from 1.73 ($\pm$0.03) to 2.23 ($\pm$0.03) as the chamber temperature increased. This result implies a temperature-mediated increase in particle-phase oxidized species. On the contrary, only a small increase in the $f_{44}$ / $f_{43}$ ratio, from 1.93 ($\pm$0.03) to 2.03 ($\pm$0.03), was observed during the control experiment, which implies that the SOA composition in this experiment remained relatively constant.

### 3.4 Effect of phase partitioning on SOA properties

During the aging of SOAs by photolysis with increasing temperature, we observed a decrease of the mass concentration (Fig. 1) which was associated with an increase of the $f_{44}$ / $f_{43}$ ratio of bulk particles (Fig. 6b). These evolutions may result from possible shifts of some semi-volatile organics to the gas phase as temperature increases. A second possible explanation would be the photochemical reactions that occur in the condensed phase combined with the evaporation of less oxidized compounds. In this case, photolysis could lead to a loss of semi-volatile and less oxidized compounds in the particle phase due to the fragmentation of condensed-phase species (Donahue et al., 2012; Henry and Donahue, 2012).

In order to investigate if the increase in temperature can explain the SOA mass decrease, the SOA formation and evolution were modelled with the detailed chemical schemes GECKO-A and MCM. In these models, the simulated SOA formation started at the initial step of $\alpha$-pinene ozonolysis. The effects of temperature on phase partitioning were simulated with both models. The effects of photochemical reactions and heterogeneous reactions by $O_3$ were ignored in these simulations. As shown in Fig. 7 for the initial SOA formation period, the time profiles of $\alpha$-pinene and ozone concentrations were well reproduced by both models within the measurement uncertainties. Although the temporal profile of the SOA formation was also well reproduced by the models, the simulated mass concentrations of SOAs obtained using the GECKO-A and MCM models (302 and 337 $\mu g\,m^{-3}$, respectively) were higher than those observed in the experiment (130 $\mu g\,m^{-3}$). This overestimation of the simulated SOA mass concentration might be due either to an underestimation of the vapour pressure with the Nannoolal method used in this study or some oxidation processes occurring in the aerosol phase and leading to fragmentation not implemented in the model. In addition, an unavoidable consequence of simulation chamber measurements is the interaction of gases with the chamber wall surfaces. It is plausible that the VOC-wall losses affect the SOA mass concentration by being a sink for semi-volatile products preventing them from condensing on the aerosol phase.

Four experiments, each of which exhibited different temperature increases, were simulated using these models. SOA mass concentration loss was calculated as the difference between the mass concentration before and after each forcing. For the simulations, only the effects of the temperature on phase partitioning were simulated with both models. The effects of photochemical reaction on the gas and particle phase were omitted. A comparison between the observed and modelled loss of SOA mass concentration under these temperature conditions is presented in Fig. 8a. As shown in this figure, both the temporal profile and magnitude of SOA mass loss observed in these experiments were well reproduced by the GECKO-A and MCM models. This finding suggests that the observed heating-induced loss in SOA mass concentration can be explained by the temperature-dependent gas–particle phase partitioning of the semi-volatile components of SOA.

The measured and simulated O : C ratios for these experiments are shown in Fig. 8b. Before the forcing, both models predict an O : C ratio of 0.49, which is within the uncer-

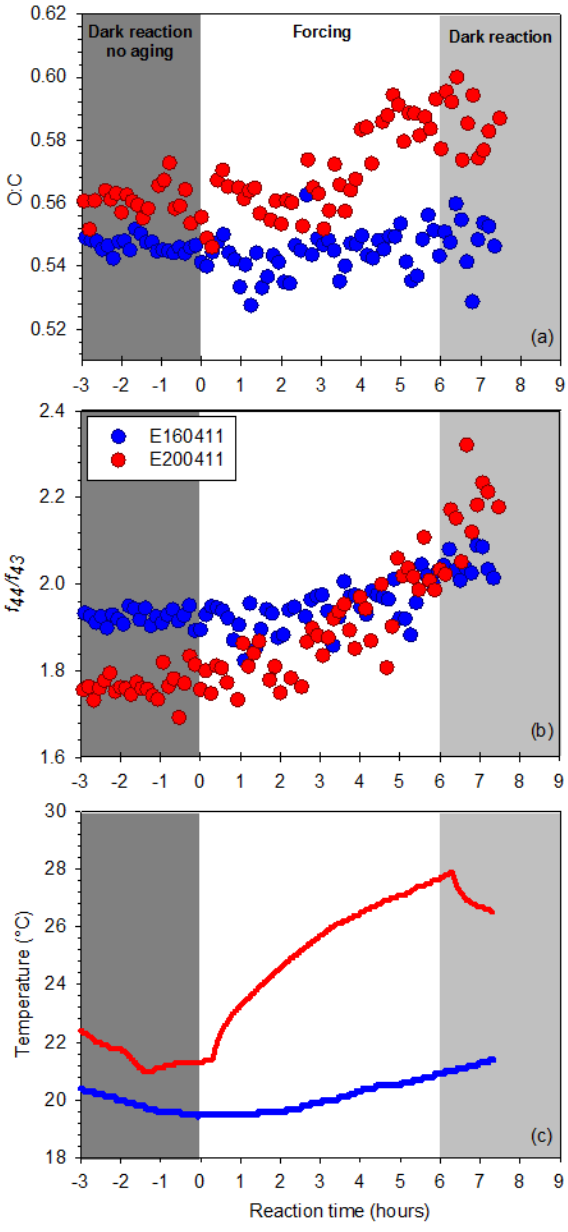


**Figure 6.** Evolution of the **(a)** O : C ratio and **(b)** $f_{44}/f_{43}$ ratio of SOAs during the control experiment (blue circles) and during exposure to light with increasing temperature (red circles). The temperature profiles within the chamber during the two experiments are shown in **(c)**. Here, the initial time $t = 0$ corresponds to the beginning of simulated aging, which was commenced after SOA was allowed to form and stabilize for 14 h.

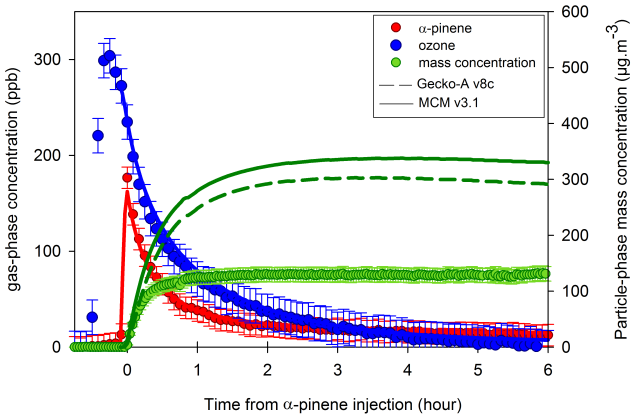


**Figure 7.** Comparison of temporal profiles of measured $\alpha$-pinene (red circles), ozone (blue circles) and SOA mass concentration (green circles) with those modelled using GECKO-A (dashed lines) and the master chemical mechanism (MCM) (solid lines). The experimental data are taken from experiment E160410.

tainty of the experimental value ($0.55 \pm 0.16$) obtained with the AMS. During the aging experiments, the O : C ratio simulated with the two models increased with increasing temperature; for example, experiment E200411, which showed the highest temperature increase (+6.5 °C; red in Fig. 8c), also showed the highest increase in simulated O : C ratio (from 0.49 to 0.51); on the contrary, experiment E060512 exhibited constant values for both temperature and simulated O : C ratio (yellow in Fig. 8b and c). These results suggest that the changes in SOA physical and chemical properties observed in these experiments resulted from the heating-induced evaporation of semi-volatile and less oxidized SOA species, which in turn modified the optical and hygroscopic properties of the condensed phase.

## 4 Discussion

Our results have shown that exposure of SOAs to increasing temperature enhances its hydrophilicity, degree of oxidation and scattering properties. On the contrary, the few previous studies investigating the changes in physical and chemical properties of $\alpha$-pinene–$O_3$ SOAs as a function of temperature have largely found little effect: Cappa and Wilson (2011) observed a reduction in the total mass concentration but no change in the mass spectra of $\alpha$-pinene–$O_3$ SOAs after heating at 170 °C, and Kim and Paulson (2013) showed no significant change over temperatures ranging from 23 to 86 °C in the real CRI of SOAs. Using AMS data, Huffman et al. (2009) observed an increase in SOA oxygen content during SOA evaporation. This trend is in good agreement with the increase in the $CO_2^+$ fragment ($m/z$ 44) with SOA evaporation observed by Kostenidou et al. (2009). Finally, Warren et al. (2009) showed that the GF of SOAs decreased with decreasing temperature from 27 °C to 5 °C. These disagreements with the present study may be attributable to two differences in experimental conditions. First, in the present study, the long timescale of the experiments (20 h) allows for stability in the chemical composition of the semi-volatile component of SOAs before processing. On the contrary, in the previous studies, SOA volatility was measured only several minutes after its formation. Since the chemical composi-

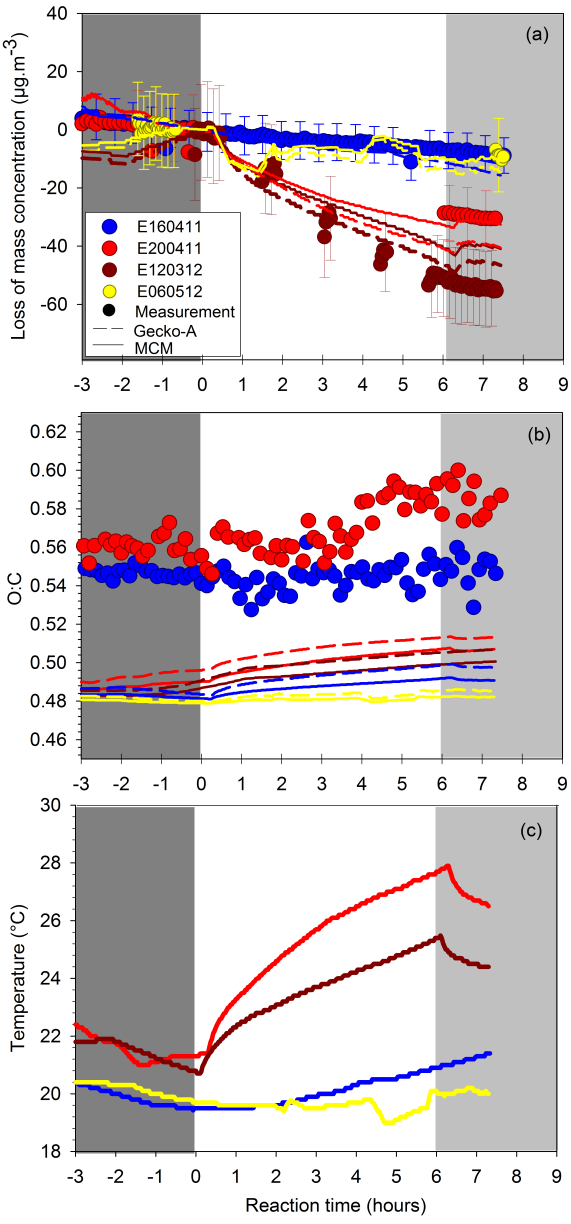


**Figure 8. (a)** Loss in SOA mass concentration (calculated as the difference between the SOA mass concentrations before and after simulated atmospheric processing) and **(b)** O : C ratio of the bulk SOAs for four experiments exhibiting **(c)** different temperature increases. Here, the experimental data (filled circles) are compared with results obtained using the MCM (solid lines) and the GECKO-A (dashed lines) models. The blue points refer to the control experiment (E160411), the yellow points refer to an experiment in which SOA was exposed to light under controlled temperature conditions (E060512), and the red and brown points refer to experiments in which SOA was exposed to light and increasing temperature (E200411; E120312). Here, the initial time $t = 0$ corresponds to the beginning of simulated aging, which was commenced after SOA was allowed to form and stabilize for 14 h.

tion of SOAs has been observed to vary significantly during its formation (Shilling et al., 2008; Chhabra et al., 2010; Denjean et al., 2014b), it is likely that the volatility of the condensed species also varies during this time period. Second, in most of the previous studies, temperature variation was performed using a thermodenuder. The timescale for aerosol evaporation within thermodenuders ($\sim$ 16 s) is significantly lower than in simulation chambers (several hours) and, owing to mass transfer limitations, may not be long enough for SOA evaporation to occur (Lee et al., 2011).

Surprisingly, our results suggest that exposure of $\alpha$-pinene SOAs to light and $O_3$ does not significantly change its chemical, hygroscopic and optical properties. These observations suggest that, under our experimental conditions, neither significant photolysis nor ozonolysis of the particle-phase products occurred.

Several previous studies have reported a decline in $\alpha$-pinene–$O_3$ SOA mass after irradiation under exposure to low OH concentrations (Donahue et al., 2012; Henry and Donahue, 2012). These authors used UV lights ($\sim$ 360 nm) to initiate photochemistry; on the contrary, a more realistic reproduction of the solar energy distribution at the Earth's surface was used in our study (Wang et al., 2011). In a test of the effect of light source upon SOA aging, Donahue et al. (2012) observed a monotonic decrease in SOA mass during aging with 360 nm UV lights, but an increase in SOA mass during aging with sunlight or quasi-solar lamps. These observations can be explained by the fact that some oxygenated organics in the SOA condensed phase, such as carbonyls or peroxides, undergo photodissociation by photolysis at the specific wavelength of 360 nm. Together, these results highlight the strong influence of the light source on the photodissociation of SOAs, and underscore the utility of experiments performed under realistic illumination conditions.

In addition, the molecular structure of $\alpha$-pinene, which contains only one double bond and thus one active site for ozone reaction, limits the gas-phase oxidation by ozone of reaction products of $\alpha$-pinene. Since no scavenger of OH radicals was added, $\alpha$-pinene–$O_3$ SOA is likely a mixture of OH and $O_3$ oxidation products of $\alpha$-pinene. Therefore, some of the products may still contain unreacted C=C bonds, which can then react with $O_3$. Our results indicate that the relative contribution of the products of these reactions may not be sufficient to significantly affect the chemical properties of SOAs during the ozone-induced forcing.

Recent literature has highlighted that $\alpha$-pinene–$O_3$ SOA is not composed of a homogeneous chemical mixture. For example, when Maurin et al. (2015) exposed $\alpha$-pinene–$O_3$ SOA to high concentrations of $O_3$, they observed a constant particle-phase concentration of verbenone, an unsaturated oxygenated product. Since this molecule would have been expected to be consumed by heterogeneous reaction with $O_3$, and since heterogeneous particle-phase reactions are predicted to occur mainly at the surface of the particles (Shiraiwa et al., 2013), these authors postulated that reaction

of $O_3$ with verbenone was kinetically limited by the diffusion of buried verbenone to the particle surface. This hypothesis is also supported by our observation that $\alpha$-pinene–$O_3$ SOA exhibits a core-shell structure, with less oxidized species at its surface (Denjean et al., 2014b). The effect of the forcing would depend not only on the chemical composition of the bulk particle, but also on the chemical surface and the phase of the particle.

## 5 Conclusions

We have demonstrated that the size, chemical composition, hygroscopicity and optical properties of $\alpha$-pinene–$O_3$ SOAs change dramatically in response to relatively minor increases in temperature ($\sim 6\,^{\circ}C$). These changes, in turn, have implications for the role that SOA plays in climate. For example, the volatilization-induced increase in the real part of the SOA CRI is likely to enhance the direct radiative effect of SOA by increasing its ability to scatter radiation. The direct radiative effect of SOA can be parameterized using the mass extinction efficiency $k_{ext}$ at 525 nm, which is defined as the ratio of the measured $\sigma_{scat}$ at 525 nm to the SOA mass concentration. In our companion paper (Denjean et al. 2014b), we have estimated a value of $k_{ext} = 1.7 \pm 0.5\,m^2\,g^{-1}$ for unprocessed SOAs. In the present experiments, we estimate a value of $k_{ext} = 2.8 \pm 0.5\,m^2\,g^{-1}$ for SOAs exposed to light and temperature increase, which implies that this aging regime led to a $\sim 40\,\%$ enhancement in this parameter. We attribute this enhancement to both the decrease in SOA particle size and the increase in the scattering component of the CRI upon heating.

As shown in this work, exposure of SOAs to increasing temperature also leads to an increase in SOA hygroscopicity: the SOA GF increased from 1.04 to 1.14 as a result of this forcing. In order to estimate the influence of these changes in hygroscopicity on the direct radiative effect of SOAs, we made the simplified assumption that SOA exhibits a homogeneous mixing state with water. We used Mie scattering calculations for homogeneous spheres to determine $\sigma_{scat}$ at 90 % RH both from the measured GF and the CRI. The CRI calculations were based on volume-weighted CRI of values of $\alpha$-pinene–$O_3$ SOA and water. We estimate that $k_{ext}$ (90 % RH) $= 2.8 \pm 0.7\,m^2\,g^{-1}$ after SOA volatilization, which is significantly higher than the value of $k_{ext}$ (90 % RH) $= 2.3 \pm 0.7\,m^2\,g^{-1}$ calculated in Denjean et al. (2014b) for unprocessed SOAs. Since we have shown that volatilization of condensed-phase species takes place over a range of temperatures consistent with diurnal fluctuations, we suggest that these changes in $k_{ext}$ are representative of the diurnal evolution of SOAs during its lifetime in the atmosphere.

Our results also suggest that $\alpha$-pinene–$O_3$ SOA is quite insensitive to light- and ozone-induced aging under our experimental conditions. Insensitivity to ozone-induced aging is most likely a result of the molecular structure of $\alpha$-pinene which limit the gas-phase oxidation by ozone of reaction products of $\alpha$-pinene. In addition, several recent studies have reported that $\alpha$-pinene–$O_3$ SOA undergoes a transition from a more glassy state to a more liquid state with increasing RH (Saukko et al., 2012; Renbaum-Wolff et al., 2013; Denjean et al., 2014b). On the basis of viscosity data and the Stokes–Einstein equation, Renbaum-Wolff et al. (2013) estimated that the change in $\alpha$-pinene–$O_3$ SOA viscosity associated with its transition from a solid to a semi-solid state increases the bulk diffusion coefficient of particles by 6 orders of magnitude (from $< 10^{-17}\,cm^2\,s^{-1}$ to $10^{-11}\,cm^2\,s^{-1}$). Since an increase in bulk diffusion coefficient would be expected to be accompanied by an increase in particle reactivity, we suggest that future studies examine the effect of ozone and light exposure on $\alpha$-pinene–$O_3$ SOA properties under humidified conditions (i.e. RH > 30 %). Beyond its effect on the physical state of the particles, the relative humidity may influence the chemical composition of SOAs. Recently, Kristensen et al. (2014) observed that $\alpha$-pinene–$O_3$ SOAs increased concentrations of high molecular weight compounds, such as dimer esters, at higher RH (> 50 %) relative to lower RH (< 30 %). An increase in high molecular weight compounds with increase RH could lead to a change in hygroscopic and optical properties of $\alpha$-pinene–$O_3$ SOAs as well as its sensitivity to aging processes. In addition, further experimental studies on SOAs which exhibit different viscosity are required in order to evaluate the atmospheric implication of the oxidative processing and photochemistry.

*Acknowledgements.* This research work has been supported by the European Community within the seventh Framework Program Eurochamp-2 (EU-FP7 grant agreement no. 228335). We also acknowledge the French National Research Agency (ANR) through the CUMULUS project. We thank Frank Siekmann and Sylvain Ravier (Aix-Marseille Université, France) for their help in calibrating the AMS during the measurement campaign. We thank Sarah Styler (Leibniz Institute for Tropospheric Research, Germany) for helpful revision of the manuscript.

Edited by: A. Virtanen

## References

Aiken, A. C., DeCarlo, P. F., and Jimenez, J. L.: Elemental analysis of organic species with electron ionization high-resolution mass spectrometry, Anal. Chem., 79, 8350–8358, doi:10.1021/ac071150w, 2007.

Alfarra, M. R., Good, N., Wyche, K. P., Hamilton, J. F., Monks, P. S., Lewis, A. C., and McFiggans, G.: Water uptake is independent of the inferred composition of secondary aerosols derived from multiple biogenic VOCs, Atmos. Chem. Phys., 13, 11769–11789, doi:10.5194/acp-13-11769-2013, 2013.

Allan, J. D., Delia, A. E., Coe, H., Bower, K. N., Alfarra, M. R., Jimenez, J. L., Middlebrook, A. M., Drewnick, F., Onasch, T. B.,

Canagaratna, M. R., Jayne, J. T., and Worsnop, D. R.: A generalised method for the extraction of chemically resolved mass spectra from Aerodyne aerosol mass spectrometer data, J. Aerosol Sci., 35, 909–922, doi:10.1016/j.jaerosci.2004.02.007, 2004.

Asa-Awuku, A., Engelhart, G. J., Lee, B. H., Pandis, S. N., and Nenes, A.: Relating CCN activity, volatility, and droplet growth kinetics of $\beta$-caryophyllene secondary organic aerosol, Atmos. Chem. Phys., 9, 795–812, doi:10.5194/acp-9-795-2009, 2009.

Aumont, B., Szopa, S., and Madronich, S.: Modelling the evolution of organic carbon during its gas-phase tropospheric oxidation: development of an explicit model based on a self generating approach, Atmos. Chem. Phys., 5, 2497–2517, doi:10.5194/acp-5-2497-2005, 2005.

Barley, M. H. and McFiggans, G.: The critical assessment of vapour pressure estimation methods for use in modelling the formation of atmospheric organic aerosol, Atmos. Chem. Phys., 10, 749–767, doi:10.5194/acp-10-749-2010, 2010.

Bateman, A. P., Nizkorodov, S. A., Laskin, J., and Laskin, A.: Photolytic processing of secondary organic aerosols dissolved in cloud droplets, Phys. Chem. Chem. Phys., 13, 12199–12212, doi:10.1039/c1cp20526a, 2011.

Bohren, C. F. and Huffman, D. R.: Absorption and Scattering of Light by Small Particles, Wiley, New York, 1983.

Bones, D. L., Henricksen, D. K., Mang, S. A., Gonsior, M., Bateman, A. P., Nguyen, T. B., Cooper, W. J., and Nizkorodov, S. A.: Appearance of strong absorbers and fluorophores in limonene-$O_3$ secondary organic aerosol due to NH4+-mediated chemical aging over long time scales, J. Geophys. Res. Atmos., 115, D05203, doi:10.1029/2009JD012864, 2010.

Camredon, M., Aumont, B., Lee-Taylor, J., and Madronich, S.: The SOA/VOC/$NO_x$ system: an explicit model of secondary organic aerosol formation, Atmos. Chem. Phys., 7, 5599–5610, doi:10.5194/acp-7-5599-2007, 2007.

Canagaratna, M. R., Jimenez, J. L., Kroll, J. H., Chen, Q., Kessler, S. H., Massoli, P., Hildebrandt Ruiz, L., Fortner, E., Williams, L. R., Wilson, K. R., Surratt, J. D., Donahue, N. M., Jayne, J. T., and Worsnop, D. R.: Elemental ratio measurements of organic compounds using aerosol mass spectrometry: characterization, improved calibration, and implications, Atmos. Chem. Phys. Discuss., 14, 19791–19835, doi:10.5194/acpd-14-19791-2014, 2014.

Cappa, C. D. and Wilson, K. R.: Evolution of organic aerosol mass spectra upon heating: implications for OA phase and partitioning behavior, Atmos. Chem. Phys., 11, 1895–1911, doi:10.5194/acp-11-1895-2011, 2011.

Cappa, C. D., Che, D. L., Kessler, S. H., Kroll, J. H., and Wilson, K. R.: Variations in organic aerosol optical and hygroscopic properties upon heterogeneous OH oxidation, J. Geophys. Res., 116, D15204, doi:10.1029/2011JD015918, 2011.

Carter, W. P. L., Cocker Iii, D. R., Fitz, D. R., Malkina, I. L., Bumiller, K., Sauer, C. G., Pisano, J. T., Bufalino, C., and Song, C.: A new environmental chamber for evaluation of gas-phase chemical mechanisms and secondary aerosol formation, Atmos. Environ., 39, 7768–7788, doi:10.1016/j.atmosenv.2005.08.040, 2005.

Chang, R. Y.-W., Slowik, J. G., Shantz, N. C., Vlasenko, A., Liggio, J., Sjostedt, S. J., Leaitch, W. R., and Abbatt, J. P. D.: The hygroscopicity parameter ($\kappa$) of ambient organic aerosol at a field site subject to biogenic and anthropogenic influences: relationship to degree of aerosol oxidation, Atmos. Chem. Phys., 10, 5047–5064, doi:10.5194/acp-10-5047-2010, 2010.

Chen, Q., Liu, Y. J., Donahue, N. M., Shilling, J. E., and Martin, S. T.: Particle-Phase Chemistry of Secondary Organic Material: Modeled Compared to Measured O : C and H:C Elemental Ratios Provide Constraints, Environ. Sci. Technol., 45, 4763–4770, doi:10.1021/es104398s, 2011.

Chhabra, P. S., Flagan, R. C., and Seinfeld, J. H.: Elemental analysis of chamber organic aerosol using an aerodyne high-resolution aerosol mass spectrometer, Atmos. Chem. Phys., 10, 4111–4131, doi:10.5194/acp-10-4111-2010, 2010.

Cocker, D. R., Clegg, S. L., Flagan, R. C., and Seinfeld, J. H.: The effect of water on gas-particle partitioning of secondary organic aerosol. Part I: alpha-pinene/ozone system, Atmos. Environ., 35, 6049–6072, doi:10.1016/s1352-2310(01)00404-6, 2001.

Collaud Coen, M., Weingartner, E., Apituley, A., Ceburnis, D., Fierz-Schmidhauser, R., Flentje, H., Henzing, J. S., Jennings, S. G., Moerman, M., Petzold, A., Schmid, O., and Baltensperger, U.: Minimizing light absorption measurement artifacts of the Aethalometer: evaluation of five correction algorithms, Atmos. Meas. Tech., 3, 457–474, doi:10.5194/amt-3-457-2010, 2010.

de Gouw, J. A., Middlebrook, A. M., Warneke, C., Goldan, P. D., Kuster, W. C., Roberts, J. M., Fehsenfeld, F. C., Worsnop, D. R., Canagaratna, M. R., Pszenny, A. A. P., Keene, W. C., Marchewka, M., Bertman, S. B., and Bates, T. S.: Budget of organic carbon in a polluted atmosphere: results from the New England Air Quality Study in 2002, J. Geophys. Res.-Atmos., 110, D16305, doi:10.1029/2004JD005623, 2005.

DeCarlo, P. F., Kimmel, J. R., Trimborn, A., Northway, M. J., Jayne, J. T., Aiken, A. C., Gonin, M., Fuhrer, K., Horvath, T., Docherty, K. S., Worsnop, D. R., and Jimenez, J. L.: Field-deployable, high-resolution, time-of-flight aerosol mass spectrometer, Anal. Chem., 78, 8281–8289, doi:10.1021/ac061249n, 2006.

Denjean, C., Formenti, P., Picquet-Varrault, B., Katrib, Y., Pangui, E., Zapf, P., and Doussin, J. F.: A new experimental approach to study the hygroscopic and optical properties of aerosols: application to ammonium sulfate particles, Atmos. Meas. Tech., 7, 183–197, doi:10.5194/amt-7-183-2014, 2014a.

Denjean, C., Formenti, P., Picquet-Varrault, B., Pangui, E., Zapf, P., Katrib, Y., Giorio, C., Tapparo, A., Monod, A., Temime-Roussel, B., Decorse, P., Mangeney, C., and Doussin, J. F.: Relating hygroscopicity and optical properties to chemical composition and structure of secondary organic aerosol particles generated from the ozonolysis of $\alpha$-pinene, Atmos. Chem. Phys. Discuss., 14, 10543–10596, doi:10.5194/acpd-14-10543-2014, 2014b.

Donahue, N. M., Henry, K. M., Mentel, T. F., Kiendler-Scharr, A., Spindler, C., Bohn, B., Brauers, T., Dorn, H. P., Fuchs, H., Tillmann, R., Wahner, A., Saathoff, H., Naumann, K. H., Mohler, O., Leisner, T., Muller, L., Reinnig, M. C., Hoffmann, T., Salo, K., Hallquist, M., Frosch, M., Bilde, M., Tritscher, T., Barmet, P., Praplan, A. P., DeCarlo, P. F., Dommen, J., Prevot, A. S. H., and Baltensperger, U.: Aging of biogenic secondary organic aerosol via gas-phase OH radical reactions, P. Natl. Acad. Sci. USA, 109, 13503–13508, doi:10.1073/pnas.1115186109, 2012.

Duplissy, J., DeCarlo, P. F., Dommen, J., Alfarra, M. R., Metzger, A., Barmpadimos, I., Prevot, A. S. H., Weingartner, E.,

Tritscher, T., Gysel, M., Aiken, A. C., Jimenez, J. L., Canagaratna, M. R., Worsnop, D. R., Collins, D. R., Tomlinson, J., and Baltensperger, U.: Relating hygroscopicity and composition of organic aerosol particulate matter, Atmos. Chem. Phys., 11, 1155–1165, doi:10.5194/acp-11-1155-2011, 2011.

Ellison, G. B., Tuck, A. F., and Vaida, V.: Atmospheric processing of organic aerosols, J. Geophys. Res.-Atmos., 104, 11633–11641, doi:10.1029/1999jd900073, 1999.

Ervens, B. and Volkamer, R.: Glyoxal processing by aerosol multiphase chemistry: towards a kinetic modeling framework of secondary organic aerosol formation in aqueous particles, Atmos. Chem. Phys., 10, 8219–8244, doi:10.5194/acp-10-8219-2010, 2010.

Flores, J. M., Zhao, D. F., Segev, L., Schlag, P., Kiendler-Scharr, A., Fuchs, H., Watne, Å. K., Bluvshtein, N., Mentel, Th. F., Hallquist, M., and Rudich, Y.: Evolution of the complex refractive index in the UV spectral region in ageing secondary organic aerosol, Atmos. Chem. Phys., 14, 5793–5806, doi:10.5194/acp-14-5793-2014, 2014.

Gao, S., Ng, N. L., Keywood, M., Varutbangkul, V., Bahreini, R., Nenes, A., He, J., Yoo, K. Y., Beauchamp, J. L., Hodyss, R. P., Flagan, R. C., and Seinfeld, J. H.: Particle phase acidity and oligomer formation in secondary organic aerosol, Environ. Sci. Technol., 38, 6582–6589, doi:10.1021/es049125k, 2004.

George, I. J., Chang, R. Y. W., Danov, V., Vlasenko, A., and Abbatt, J. P. D.: Modification of cloud condensation nucleus activity of organic aerosols by hydroxyl radical heterogeneous oxidation, Atmos. Environ., 43, 5038–5045, doi:10.1016/j.atmosenv.2009.06.043, 2009.

George, I. J. and Abbatt, J. P. D.: Chemical evolution of secondary organic aerosol from OH-initiated heterogeneous oxidation, Atmos. Chem. Phys., 10, 5551–5563, doi:10.5194/acp-10-5551-2010, 2010.

Guenther, A., Hewitt, C. N., Erickson, D., Fall, R., Geron, C., Graedel, T., Harley, P., Klinger, L., Lerdau, M., Mckay, W. A., Pierce, T., Scholes, B., Steinbrecher, R., Tallamraju, R., Taylor, J., and Zimmerman, P.: A global model of natural volatile organic compound emissions, J. Geophys. Res., 100, 8873–8892, doi:10.1029/94JD02950, 1995.

Hallquist, M., Wenger, J. C., Baltensperger, U., Rudich, Y., Simpson, D., Claeys, M., Dommen, J., Donahue, N. M., George, C., Goldstein, A. H., Hamilton, J. F., Herrmann, H., Hoffmann, T., Iinuma, Y., Jang, M., Jenkin, M. E., Jimenez, J. L., Kiendler-Scharr, A., Maenhaut, W., McFiggans, G., Mentel, Th. F., Monod, A., Prévôt, A. S. H., Seinfeld, J. H., Surratt, J. D., Szmigielski, R., and Wildt, J.: The formation, properties and impact of secondary organic aerosol: current and emerging issues, Atmos. Chem. Phys., 9, 5155–5236, doi:10.5194/acp-9-5155-2009, 2009.

Hawkins, L. N. and Russell, L. M.: Oxidation of ketone groups in transported biomass burning aerosol from the 2008 Northern California Lightning Series fires, Atmos. Environ., 44, 4142–4154, doi:10.1016/j.atmosenv.2010.07.036, 2010.

Haywood, J. M. and Ramaswamy, V.: Global sensitivity studies of the direct radiative forcing due to anthropogenic sulfate and black carbon aerosols, J. Geophys. Res.-Atmos., 103, 6043–6058, doi:10.1029/97JD03426, 1998.

Henry, K. M. and Donahue, N. M.: Photochemical aging of alpha-pinene secondary organic aerosol: effects of oh radical sources and photolysis, J. Phys. Chem. A, 116, 5932–5940, doi:10.1021/jp210288s, 2012.

Huffman, J. A., Docherty, K. S., Mohr, C., Cubison, M. J., Ulbrich, I. M., Ziemann, P. J., Onasch, T. B., and Jimenez, J. L.: Chemically-resolved volatility measurements of organic aerosol from different sources, Environ. Sci. Technol., 43, 5351–5357, doi:10.1021/es803539d, 2009.

Jimenez, J. L., Canagaratna, M. R., Donahue, N. M., Prevot, A. S. H., Zhang, Q., Kroll, J. H., DeCarlo, P. F., Allan, J. D., Coe, H., Ng, N. L., Aiken, A. C., Docherty, K. S., Ulbrich, I. M., Grieshop, A. P., Robinson, A. L., Duplissy, J., Smith, J. D., Wilson, K. R., Lanz, V. A., Hueglin, C., Sun, Y. L., Tian, J., Laaksonen, A., Raatikainen, T., Rautiainen, J., Vaattovaara, P., Ehn, M., Kulmala, M., Tomlinson, J. M., Collins, D. R., Cubison, M. J., E., Dunlea, J., Huffman, J. A., Onasch, T. B., Alfarra, M. R., Williams, P. I., Bower, K., Kondo, Y., Schneider, J., Drewnick, F., Borrmann, S., Weimer, S., Demerjian, K., Salcedo, D., Cottrell, L., Griffin, R., Takami, A., Miyoshi, T., Hatakeyama, S., Shimono, A., Sun, J. Y., Zhang, Y. M., Dzepina, K., Kimmel, J. R., Sueper, D., Jayne, J. T., Herndon, S. C., Trimborn, A. M., Williams, L. R., Wood, E. C., Middlebrook, A. M., Kolb, C. E., Baltensperger, U., and Worsnop, D. R.: Evolution of organic aerosols in the atmosphere, Science, 326, 1525–1529, doi:10.1126/science.1180353, 2009.

Kalberer, M., Paulsen, D., Sax, M., Steinbacher, M., Dommen, J., Prevot, A. S. H., Fisseha, R., Weingartner, E., Frankevich, V., Zenobi, R., and Baltensperger, U.: Identification of polymers as major components of atmospheric organic aerosols, Science, 303, 1659–1662, doi:10.1126/science.1092185, 2004.

Kanakidou, M., Seinfeld, J. H., Pandis, S. N., Barnes, I., Dentener, F. J., Facchini, M. C., Van Dingenen, R., Ervens, B., Nenes, A., Nielsen, C. J., Swietlicki, E., Putaud, J. P., Balkanski, Y., Fuzzi, S., Horth, J., Moortgat, G. K., Winterhalter, R., Myhre, C. E. L., Tsigaridis, K., Vignati, E., Stephanou, E. G., and Wilson, J.: Organic aerosol and global climate modelling: a review, Atmos. Chem. Phys., 5, 1053–1123, doi:10.5194/acp-5-1053-2005, 2005.

Kim, H. and Paulson, S. E.: Real refractive indices and volatility of secondary organic aerosol generated from photooxidation and ozonolysis of limonene, $\alpha$-pinene and toluene, Atmos. Chem. Phys., 13, 7711–7723, doi:10.5194/acp-13-7711-2013, 2013.

Kristensen, K., Cui, T., Zhang, H., Gold, A., Glasius, M., and Surratt, J. D.: Dimer esters in $\alpha$-pinene secondary organic aerosol: effect of hydroxyl radical, ozone, relative humidity and aerosol acidity, Atmos. Chem. Phys. Discuss., 13, 32529–32574, doi:10.5194/acpd-13-32529-2013, 2013.

Kostenidou, E., Lee, B. H., Engelhart, G. J., Pierce, J. R., and Pandis, S. N.: Mass spectra deconvolution of low, medium, and high volatility biogenic secondary organic aerosol, Environ. Sci. Technol., 43, 4884–4889, doi:10.1021/es803676g, 2009.

Kourtchev, I., Fuller, S. J., Giorio, C., Healy, R. M., Wilson, E., O'Connor, I., Wenger, J. C., McLeod, M., Aalto, J., Ruuskanen, T. M., Maenhaut, W., Jones, R., Venables, D. S., Sodeau, J. R., Kulmala, M., and Kalberer, M.: Molecular composition of biogenic secondary organic aerosols using ultrahigh-resolution mass spectrometry: comparing laboratory and field studies, Atmos. Chem. Phys., 14, 2155–2167, doi:10.5194/acp-14-2155-2014, 2014.

Kroll, J. H. and Seinfeld, J. H.: Chemistry of secondary organic aerosol: formation and evolution of low-volatility organics in the atmosphere, Atmos. Environ., 42, 3593–3624, doi:10.1016/j.atmosenv.2008.01.003, 2008.

Kroll, J. H., Ng, N. L., Murphy, S. M., Flagan, R. C., and Seinfeld, J. H.: Secondary organic aerosol formation from isoprene photooxidation, Environ. Sci. Technol., 40, 1869–1877, doi:10.1021/es0524301, 2006.

Lambe, A. T., Cappa, C. D., Massoli, P., Onasch, T. B., Forestieri, S. D., Martin, A. T., Cummings, M. J., Croasdale, D. R., Brune, W. H., Worsnop, D. R., and Davidovits, P.: Relationship between oxidation level and optical properties of secondary organic aerosol, Environ. Sci. Technol., 47, 6349–6357, doi:10.1021/es401043j, 2013.

Laskin, J., Laskin, A., Roach, P. J., Slysz, G. W., Anderson, G. A., Nizkorodov, S. A., Bones, D. L., and Nguyen, L. Q.: High-Resolution Desorption Electrospray Ionization Mass Spectrometry for Chemical Characterization of Organic Aerosols, Analyt. Chem., 82, 2048–2058, doi:10.1021/ac902801f, 2010.

Lee, B.-H., Pierce, J. R., Engelhart, G. J., and Pandis, S. N.: Volatility of secondary organic aerosol from the ozonolysis of monoterpenes, Atmos. Environ., 45, 2443–2452, doi:10.1016/j.atmosenv.2011.02.004, 2011.

Li, Y. P., Elbern, H., Lu, K. D., Friese, E., Kiendler-Scharr, A., Mentel, Th. F., Wang, X. S., Wahner, A., and Zhang, Y. H.: Updated aerosol module and its application to simulate secondary organic aerosols during IMPACT campaign May 2008, Atmos. Chem. Phys., 13, 6289–6304, doi:10.5194/acp-13-6289-2013, 2013.

Liu, Y. G. and Daum, P. H.: Relationship of refractive index to mass density and self-consistency of mixing rules for multicomponent mixtures like ambient aerosols, J. Aerosol Sci., 39, 974–986, doi:10.1016/j.jaerosci.2008.06.006, 2008.

Lohmann, U. and Feichter, J.: Global indirect aerosol effects: a review, Atmos. Chem. Phys., 5, 715–737, doi:10.5194/acp-5-715-2005, 2005.

Massoli, P., Lambe, A. T., Ahern, A. T., Williams, L. R., Ehn, M., Mikkilä, J., Canagaratna, M. R., Brune, W. H., Onasch, T. B., Jayne, J. T., Petäjä, T., Kulmala, M., Laaksonen, A., Kolb, C. E., Davidovits, P., and Worsnop, D. R.: Relationship between aerosol oxidation level and hygroscopic properties of laboratory generated secondary organic aerosol (SOA) particles, Geophys. Res. Lett., 37, L24801, doi:10.1029/2010GL045258, 2010.

Maurin, N., Perraudin, E., Buzinski, H., Pardon, P., Pangui, E., and Doussin, J.-F.: Chemical composition and aging at the molecular level of secondary organic aerosol formed from ozonolysis of $\alpha$-pinene – Part 2: effect of aging induced by ozone, light and humidity, Atmos. Chem. Phys. Discuss., in preparation, 2015.

Nakayama, T., Matsumi, Y., Sato, K., Imamura, T., Yamazaki, A., and Uchiyama, A.: Laboratory studies on optical properties of secondary organic aerosols generated during the photooxidation of toluene and the ozonolysis of alpha-pinene, J. Geophys. Res.-Atmos., 115, doi:10.1029/2010jd014387, 2010.

Nannoolal, Y., Rarey, J., Ramjugernath, D., and Cordes, W.: Estimation of pure component properties Part 1. Estimation of the normal boiling point of non-electrolyte organic compounds via group contributions and group interactions, Fluid Phase Equilibr., 226, 45–63, doi:10.1016/j.fluid.2004.09.001, 2004.

Nannoolal, Y., Rarey, J., and Ramjugernath, D.: Estimation of pure component properties – Part 3. Estimation of the vapor pressure of non-electrolyte organic compounds via group contributions and group interactions, Fluid Phase Equilibr., 269, 117–133, doi:10.1016/j.fluid.2008.04.020, 2008.

Ng, N. L., Canagaratna, M. R., Zhang, Q., Jimenez, J. L., Tian, J., Ulbrich, I. M., Kroll, J. H., Docherty, K. S., Chhabra, P. S., Bahreini, R., Murphy, S. M., Seinfeld, J. H., Hildebrandt, L., Donahue, N. M., DeCarlo, P. F., Lanz, V. A., Prévôt, A. S. H., Dinar, E., Rudich, Y., and Worsnop, D. R.: Organic aerosol components observed in Northern Hemispheric datasets from Aerosol Mass Spectrometry, Atmos. Chem. Phys., 10, 4625–4641, doi:10.5194/acp-10-4625-2010, 2010.

Ng, N. L., Canagaratna, M. R., Jimenez, J. L., Chhabra, P. S., Seinfeld, J. H., and Worsnop, D. R.: Changes in organic aerosol composition with aging inferred from aerosol mass spectra, Atmos. Chem. Phys., 11, 6465–6474, doi:10.5194/acp-11-6465-2011, 2011.

Nozière, B. and Esteve, W.: Organic reactions increasing the absorption index of atmospheric sulfuric acid aerosols, Geophys. Res. Lett., 32, L03812, doi:10.1029/2004GL021942, 2005.

Pankow, J. F. and Asher, W. E.: SIMPOL.1: a simple group contribution method for predicting vapor pressures and enthalpies of vaporization of multifunctional organic compounds, Atmos. Chem. Phys., 8, 2773–2796, doi:10.5194/acp-8-2773-2008, 2008.

Pfaffenberger, L., Barmet, P., Slowik, J. G., Praplan, A. P., Dommen, J., Prévôt, A. S. H., and Baltensperger, U.: The link between organic aerosol mass loading and degree of oxygenation: an $\alpha$-pinene photooxidation study, Atmos. Chem. Phys., 13, 6493–6506, doi:10.5194/acp-13-6493-2013, 2013.

Poulain, L., Wu, Z., Petters, M. D., Wex, H., Hallbauer, E., Wehner, B., Massling, A., Kreidenweis, S. M., and Stratmann, F.: Towards closing the gap between hygroscopic growth and CCN activation for secondary organic aerosols – Part 3: Influence of the chemical composition on the hygroscopic properties and volatile fractions of aerosols, Atmos. Chem. Phys., 10, 3775–3785, doi:10.5194/acp-10-3775-2010, 2010.

Qi, L., Nakao, S., and Cocker, D. R.: Aging of secondary organic aerosol from $\alpha$-pinene ozonolysis: roles of hydroxyl and nitrate radicals, J. Air Waste Manage., 62, 1359–1369, doi:10.1080/10962247.2012.712082, 2012.

Renbaum-Wolff, L., Grayson, J. W., Bateman, A. P., Kuwata, M., Sellier, M., Murray, B. J., Shilling, J. E., Martin, S. T., and Bertram, A. K.: Viscosity of $\alpha$-pinene secondary organic material and implications for particle growth and reactivity, P. Natl. Acad. Sci. USA, 110, 8014–8019, doi:10.1073/pnas.1219548110, 2013.

Rudich, Y.: Laboratory perspectives on the chemical transformations of organic matter in atmospheric particles, Chem. Rev., 103, 5097–5124, doi:10.1021/cr020508f, 2003.

Saathoff, H., Naumann, K.-H., Möhler, O., Jonsson, Å. M., Hallquist, M., Kiendler-Scharr, A., Mentel, Th. F., Tillmann, R., and Schurath, U.: Temperature dependence of yields of secondary organic aerosols from the ozonolysis of $\alpha$-pinene and limonene, Atmos. Chem. Phys., 9, 1551–1577, doi:10.5194/acp-9-1551-2009, 2009.

Salo, K., Hallquist, M., Jonsson, Å. M., Saathoff, H., Naumann, K.-H., Spindler, C., Tillmann, R., Fuchs, H., Bohn, B., Rubach, F.,

Mentel, Th. F., Müller, L., Reinnig, M., Hoffmann, T., and Donahue, N. M.: Volatility of secondary organic aerosol during OH radical induced ageing, Atmos. Chem. Phys., 11, 11055–11067, doi:10.5194/acp-11-11055-2011, 2011.

Sareen, N., Moussa, S. G., and McNeill, V. F.: Photochemical aging of light-absorbing secondary organic aerosol material, J. Phys. Chem. A, 117, 2987–2996, doi:10.1021/jp309413j, 2013.

Saukko, E., Lambe, A. T., Massoli, P., Koop, T., Wright, J. P., Croasdale, D. R., Pedernera, D. A., Onasch, T. B., Laaksonen, A., Davidovits, P., Worsnop, D. R., and Virtanen, A.: Humidity-dependent phase state of SOA particles from biogenic and anthropogenic precursors, Atmos. Chem. Phys., 12, 7517–7529, doi:10.5194/acp-12-7517-2012, 2012.

Saunders, S. M., Jenkin, M. E., Derwent, R. G., and Pilling, M. J.: Protocol for the development of the Master Chemical Mechanism, MCM v3 (Part A): tropospheric degradation of non-aromatic volatile organic compounds, Atmos. Chem. Phys., 3, 161–180, doi:10.5194/acp-3-161-2003, 2003.

Shapiro, E. L., Szprengiel, J., Sareen, N., Jen, C. N., Giordano, M. R., and McNeill, V. F.: Light-absorbing secondary organic material formed by glyoxal in aqueous aerosol mimics, Atmos. Chem. Phys., 9, 2289–2300, doi:10.5194/acp-9-2289-2009, 2009.

Shilling, J. E., Chen, Q., King, S. M., Rosenoern, T., Kroll, J. H., Worsnop, D. R., McKinney, K. A., and Martin, S. T.: Particle mass yield in secondary organic aerosol formed by the dark ozonolysis of $\alpha$-pinene, Atmos. Chem. Phys., 8, 2073–2088, doi:10.5194/acp-8-2073-2008, 2008.

Shiraiwa, M., Yee, L. D., Schilling, K. A., Loza, C. L., Craven, J. S., Zuend, A., Ziemann, P. J., and Seinfeld, J. H.: Size distribution dynamics reveal particle-phase chemistry in organic aerosol formation, P. Natl. Acad. Sci. USA, 110, 11746–11750, doi:10.1073/pnas.1307501110, 2013.

Smith, J. D., Kroll, J. H., Cappa, C. D., Che, D. L., Liu, C. L., Ahmed, M., Leone, S. R., Worsnop, D. R., and Wilson, K. R.: The heterogeneous reaction of hydroxyl radicals with submicron squalane particles: a model system for understanding the oxidative aging of ambient aerosols, Atmos. Chem. Phys., 9, 3209–3222, doi:10.5194/acp-9-3209-2009, 2009.

Tritscher, T., Dommen, J., DeCarlo, P. F., Gysel, M., Barmet, P. B., Praplan, A. P., Weingartner, E., Prévôt, A. S. H., Riipinen, I., Donahue, N. M., and Baltensperger, U.: Volatility and hygroscopicity of aging secondary organic aerosol in a smog chamber, Atmos. Chem. Phys., 11, 11477–11496, doi:10.5194/acp-11-11477-2011, 2011.

Turpin, B. J. and Huntzicker, J. J.: Identification of secondary organic aerosol episodes and quantitation of primary and secondary organic aerosol concentrations during SCAQS, Atmos. Environ., 29, 3527–3544, doi:10.1016/1352-2310(94)00276-q, 1995.

Valorso, R., Aumont, B., Camredon, M., Raventos-Duran, T., Mouchel-Vallon, C., Ng, N. L., Seinfeld, J. H., Lee-Taylor, J., and Madronich, S.: Explicit modelling of SOA formation from $\alpha$-pinene photooxidation: sensitivity to vapour pressure estimation, Atmos. Chem. Phys., 11, 6895–6910, doi:10.5194/acp-11-6895-2011, 2011.

Verwer, J. G. and Vanloon, M.: An evaluation of explicit pseudo-steady-state approximation schemes for stiff ode systems from chemical-kinetics, J. Comput. Phys., 113, 347–352, 1994.

Verwer, J. G., Blom, J. G., and Hundsdorfer, W.: An implicit explicit approach for atmospheric transport-chemistry problems, Appl. Numer. Math., 20, 191–209, doi:10.1016/0168-9274(95)00126-3, 1996.

Volkamer, R., Ziemann, P. J., and Molina, M. J.: Secondary Organic Aerosol Formation from Acetylene ($C_2H_2$): seed effect on SOA yields due to organic photochemistry in the aerosol aqueous phase, Atmos. Chem. Phys., 9, 1907–1928, doi:10.5194/acp-9-1907-2009, 2009.

Wagstrom, K. M. and Pandis, S. N.: Determination of the age distribution of primary and secondary aerosol species using a chemical transport model, J. Geophys. Res.: Atmospheres, 114, D14303, doi:10.1029/2009JD011784, 2009.

Wang, J., Doussin, J. F., Perrier, S., Perraudin, E., Katrib, Y., Pangui, E., and Picquet-Varrault, B.: Design of a new multi-phase experimental simulation chamber for atmospheric photosmog, aerosol and cloud chemistry research, Atmos. Meas. Tech., 4, 2465–2494, doi:10.5194/amt-4-2465-2011, 2011.

Warren, B., Austin, R. L., and Cocker III, D. R.: Temperature dependence of secondary organic aerosol, Atmos. Environ., 43, 3548–3555, doi:10.1016/j.atmosenv.2009.04.011, 2009.

Weingartner, E., Saathoff, H., Schnaiter, M., Streit, N., Bitnar, B., and Baltensperger, U.: Absorption of light by soot particles: determination of the absorption coefficient by means of aethalometers, J. Aerosol Sci., 34, 1445–1463, doi:10.1016/S0021-8502(03)00359-8, 2003.

Yasmeen, F., Vermeylen, R., Maurin, N., Perraudin, E., Doussin, J. F., and Claeys, M.: Characterisation of tracers for aging of alpha-pinene secondary organic aerosol using liquid chromatography/negative ion electrospray ionisation mass spectrometry, Environ. Chem., 9, 236–246, doi:10.1071/en11148, 2012.

Zhang, Q., Jimenez, J. L., Canagaratna, M. R., Allan, J. D., Coe, H., Ulbrich, I., Alfarra, M. R., Takami, A., Middlebrook, A. M., Sun, Y. L., Dzepina, K., Dunlea, E., Docherty, K., DeCarlo, P. F., Salcedo, D., Onasch, T., Jayne, J. T., Miyoshi, T., Shimono, A., Hatakeyama, S., Takegawa, N., Kondo, Y., Schneider, J., Drewnick, F., Borrmann, S., Weimer, S., Demerjian, K., Williams, P., Bower, K., Bahreini, R., Cottrell, L., Griffin, R. J., Rautiainen, J., Sun, J. Y., Zhang, Y. M., and Worsnop, D. R.: Ubiquity and dominance of oxygenated species in organic aerosols in anthropogenically-influenced Northern Hemisphere midlatitudes, Geophys. Res. Lett., 34, L13801, doi:10.1029/2007gl029979, 2007.

Zhong, M., Jang, M., Oliferenko, A., Pillai, G. G., and Katritzky, A. R.: The SOA formation model combined with semiempirical quantum chemistry for predicting UV-Vis absorption of secondary organic aerosols, Phys. Chem. Chem. Phys., 14, 9058–9066, doi:10.1039/C2CP23906J, 2012.